Energy dissipation and spectrum evolution during the breaking of modulated wave trains

F. De Vita[1,2], R. Verzicco[2], A. Iafrati[1],
[1] INSEAN-CNR, Rome, Italy; [2] Univ. di Roma "Tor Vergata"
E-mail: alessandro.iafrati@cnr.it

SUMMARY In this paper the wave breaking induced by modulational instability is investigated numerically. The wave train is composed by a fundamental component with two sideband disturbances and the analysis is performed for those conditions in which the instability leads the limiting steepness to be exceeded. Due to the different speeds characterizing individual waves and the peak of the envelope, the breaking is recurrent and several breaking events are found. The study is focused on the quantification of the initial energy fraction dissipated by the entire breaking process and on the changes operated by the breaking to the initial spectrum.

1. INTRODUCTION

Free surface waves break when the steepness reaches some limiting values. There are several phenomena which can make this happen, e.g. wind-wave and wave-current interactions, shoaling effects, modulation of long waves operated by shorter ones, among others. In typical background deep-water oceanic conditions for dominant waves, however, these processes are two: linear superposition and modulational instability (Babanin *et al.*, 2011).

Due to the complexity of field measurements, detailed experimental studies of the breaking process have been mainly done in laboratory (Perlin *et al.*, 2013). Most of the studies investigate the breaking induced by the dispersive focusing technique, e.g. (Rapp & Melville, 1990; Drazen *et al.*, 2008; Grue *et al.*, 2003) among many others. In this way the breaking occurs at the focusing point as one single event. This is not the case of the wave breaking taking place in open ocean, for which recurrence is observed (Donelan *et al.*, 1972; Lamont-Smith *et al.*, 2003) as a consequence of the interaction of the peak wave component with the group envelope. The generation of such breaking in laboratory is hampered by the quite long distances needed for the development of the modulational instability. Moreover, even if the first breaking event can be generated, the limited lengths of wave tanks do not allow to follow the breaking process up to the end.

The energy dissipation and the spectrum changes associated to the breaking are very important for wave forecasting models operating on large scales (e.g. Xiao *et al.*, 2013). In order to investigate those aspects, in previous studies the breaking generated by modulational instability was simulated numerically (Iafrati *et al.*, 2012; 2013; 2014). The recurrence of the breaking process was observed and the energy amount dissipated by single breaking events was quantified for some conditions. However, not all simulations performed arrived at the end of the breaking processes and thus it wasn't possible to quantify the total energy dissipation and the changes to the pre-breaking spectrum.

In this paper some analyses similar to those discussed in Iafrati *et al.* (2014) are performed. Larger initial steepnesses are considered in order to shorten the transient needed to get to the onset of the breaking. Differently from Iafrati *et al.* (2014), here the open source Gerris code is adopted which has a sharp interface treatment and rather flexible adaptive refinement capabilities, which allow an efficient use of the computational resources. The time histories of the total energy content in water as well as the corresponding evolution of the spectra and of the maximum wave steepness are shown. It is worth remarking that results presented here are based on a two-dimensional assumption. It is hoped that some preliminary results of three-dimensional simulations can be presented at the Workshop.

2. NUMERICAL SETUP

By following what was presented in a previous edition of this Workshop (Landrini *et al.*, 1998), the initial condition is composed by a fundamental wave component with two small side band disturbances, amplitude of which is one tenth of the fundamental component at the beginning of the simulation. The free surface elevation η is thus

$$\eta(x,0) = \frac{\epsilon_0}{k_0}\left[\cos(k_0 x) + 0.1\cos\left(\frac{6}{5}k_0 x\right) + 0.1\cos\left(\frac{4}{5}k_0 x\right)\right]$$

where $k_0 = 2\pi/\lambda_0$ the wave number and $\epsilon_0 = a_0 k_0$ the steepness, a_0 denoting the amplitude of the fundamental component of wavelength λ_0. The initial velocity field in the water domain is taken from linear theory as

$$\begin{aligned} u(x,0) = \epsilon_0 \Bigg[& \sqrt{\frac{g}{k_0}}\exp(k_0 y)\cos(k_0 x) \\ & + 0.1\sqrt{\frac{6}{5}}\sqrt{\frac{g}{k_0}}\exp\left(\frac{6}{5}k_0 y\right)\cos\left(\frac{6}{5}k_0 x\right) \\ & + 0.1\sqrt{\frac{4}{5}}\sqrt{\frac{g}{k_0}}\exp\left(\frac{4}{5}k_0 y\right)\cos\left(\frac{4}{5}k_0 x\right)\Bigg] \\ v(x,0) = \epsilon_0 \Bigg[& \sqrt{\frac{g}{k_0}}\exp(k_0 y)\sin(k_0 x) \\ & + 0.1\sqrt{\frac{6}{5}}\sqrt{\frac{g}{k_0}}\exp\left(\frac{6}{5}k_0 y\right)\sin\left(\frac{6}{5}k_0 x\right) \\ & + 0.1\sqrt{\frac{4}{5}}\sqrt{\frac{g}{k_0}}\exp\left(\frac{4}{5}k_0 y\right)\sin\left(\frac{4}{5}k_0 x\right)\Bigg] \quad , \end{aligned}$$

where $g = 9.81$ m s^{-2} is the gravity acceleration. Simulations are conducted for fundamental wavelength $\lambda_0 = 0.60$ m, which is used as reference value for lengths. Periodic

case	Re	*steepness*
I	10^5	0.18
II	10^5	0.20
III	10^5	0.22
IV	1455664.8	0.18
V	1455664.8	0.20
VI	1455664.8	0.22

Table 1: Simulation conditions

boundary conditions are used at the sides in the horizontal direction. The domain width is $5\lambda_0$ whereas in the vertical direction the domain spans from $y = -0.5\lambda_0$ to $y = 1.5\lambda_0$, $y = 0$ being the still water level.

Simulations are performed by using the open-source Gerris software (http://gfs.sourceforge.net) which solves the incompressible Navier-Stokes equations and has adaptive mesh refinement capabilities by using quad-octree discretization. The solver is based on a projection method and uses a multilevel Poisson solver (Popinet, 2009). The governing equations of the problem are:

$$\frac{d\mathbf{u}}{dt} = \alpha(T)\left\{-\nabla p + \nabla\cdot[\mu(T)(\nabla\mathbf{u} + \nabla\mathbf{u}^T)] + \sigma\kappa\delta_s\mathbf{n}\right\}$$

for the fluid, and:

$$\frac{d}{dt}\int_V T\,dv + \oint_S (T\mathbf{u})\cdot\mathbf{n}\,ds = 0$$

for the interface advection, where $\mathbf{u}$ and p are, respectively, the velocity field and the pressure, $\alpha = 1/\rho$, $\rho(T)$ the local fluid density, $\mu(T)$ the dynamic viscosity, T the Volume-of-fluid variable, κ the interface curvature, σ the surface tension coefficient and δ_s the Dirac distribution which is zero out of the interface.

The fluid properties are related to the VOF variable T as:

$$\rho(T) = \rho_a T + \rho_w(1-T)$$
$$\mu(T) = \mu_a\cdot T + \mu_w(1-T)$$

so that $T = 1$ in air and $T = 0$ in water. The simulations presented here refer to the following parameters: $\mu_a = 1.810\cdot10^{-5}$ N s m^{-2}, $\mu_w = 10^{-3}$ N s m^{-2}, $\rho_a = 1.25$ kg/m^3, $\rho_w = 1000$ kg/m^3 and $\sigma = 0.072$ N/m (subscripts a and w stand for air and water, respectively). Nondimensional parameters of the problem are:

$$Re = \sqrt{g\lambda_0}\frac{\rho_w\lambda_0}{\mu_w} = 1455664.8 \quad (1)$$

$$We = \sqrt{g\lambda_0}\frac{\rho_w\lambda_0}{\sigma_w} = 219.95 \quad (2)$$

where a quantity related to the phase speed, $\sqrt{g\lambda_0}$, is used as reference velocity. As a first step of the study, in order to get confidence with the computational tool and with its adaptive refinement capabilities, simulations were performed using the much lower value of $Re = 10^5$. For this case several simulations were performed and it was found that a maximum resolution of 512 point for wavelength is enough to resolve all the dissipative scales, leading to a grid of 2560x1024 points. In order to limit the computational effort, the adaptive refinement is used. The refinement is based on the gradient of the VOF function and on the vorticity. In a second step, the full Reynolds number was adopted, which required a maximum resolution of 2048 grid point for wavelength for convergence in terms of energy dissipation. The cases studied are summarized in Table 1.

3. NUMERICAL RESULTS

In order to show the dissipation of the wave energy as a result of the breaking process, the time history of the total energy in water, computed as the sum of the kinetic and potential components, is drawn in Fig. 1 for the case with initial steepness $\epsilon_0 = 0.20$. Note that the energy is nondimensionalized by using the square of the reference velocity used for the definition of the Reynolds and Weber numbers, i.e. $g\lambda_0$. The time is made nondimensional by the characteristic time $T_0 = \lambda_0/\sqrt{g\lambda_0}$. Note that, from linear theory, the wave period of the fundamental component is $\sqrt{2\pi} \simeq 2.5$ nondimensional time units.

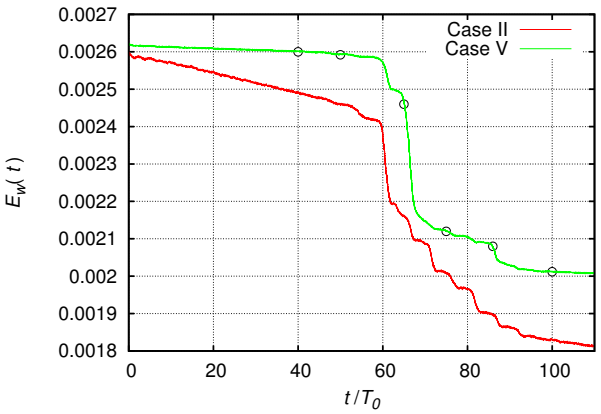

Figure 1: Time history of the total mechanical energy content in water for cases II and V.

From the time histories of the energy it can be seen that, independently of the Reynolds number, there is an initial phase during which the instability develops (see Iafrati *et al.*, 2014). During this stage the energy diminishes only due to the viscous effects associated to the orbital motion. Next, the breaking starts. As already discussed in Iafrati *et al.* (2014), the breaking is recurrent with a period which is twice the period of the fundamental wave component. This is explained as the wave crest propagates with the phase speed c_p whereas the envelop propagates with the group velocity c_g which is half of the phase speed (Lamont-Smith *et al.*, 2003).

The data in Fig. 1 indicate that the energy amount dissipated by the single breaking event can vary substantially. In terms of the total energy dissipated by the breaking process, the simulations at the two Reynolds numbers, although being characterized by a quite different decay in the pre-breaking stage, display a quite similar behavior during the

breaking process, in terms of the total energy fraction dissipated by the breaking and of duration of the process, which is about 20 wave periods in both cases. This is a quite important finding as it indicates that the scale does not play a too relevant role on those aspects, and thus makes the present result applicable to wavelengths much longer than the 0.60 m adopted here.

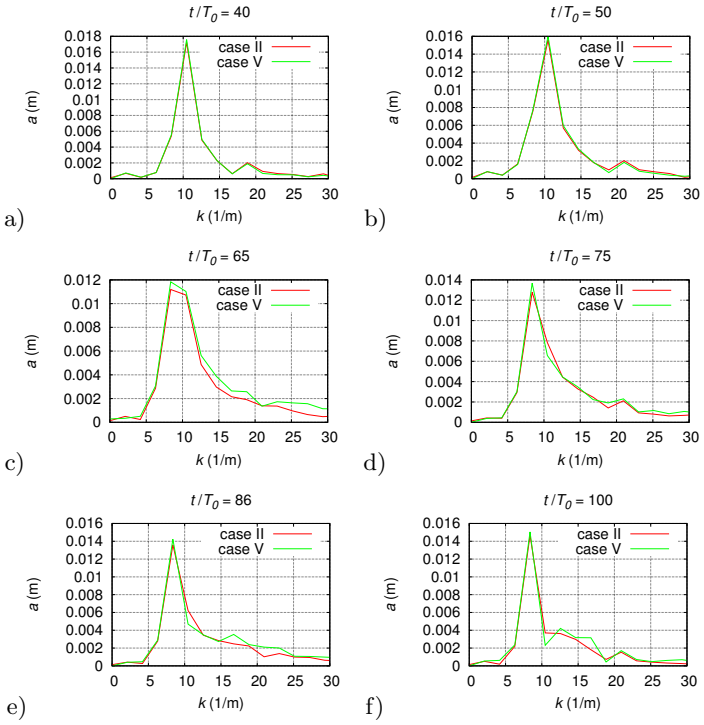

Figure 2: Comparisons of the spectra at different times during the breaking process. The figures refer to the times indicated by circles in Fig. 1. No substantial differences occur between the results at the two Reynolds numbers.

The occurrence of breaking causes a reduction of the higher wavelength components. In order to highlight the phenomenon and to provide a quantitative estimate the spectra at different phases of the breaking process are drawn in Fig. 2. The phenomenon, which was discussed on the basis of experimental data by Tulin and Waseda (1999) and was referred to as downshifting, is clearly shown also by the computational results. By comparing the spectra at the two Reynolds numbers shown in Fig. 2*c* with the corresponding energy contents at the same time shown in Fig. 1, it can be noticed that the spectra are essentially similar although the energy content is quite different. It would seem that the spectrum is mainly related to the time elapsed from the breaking on set rather than the actual energy dissipation, but the point needs a much deeper investigation. Figure 2 indicates that also in terms of the spectra, the results of the simulations at the two different Reynolds display a quite nice overlapping, despite the different dissipation rate in the pre-breaking stage.

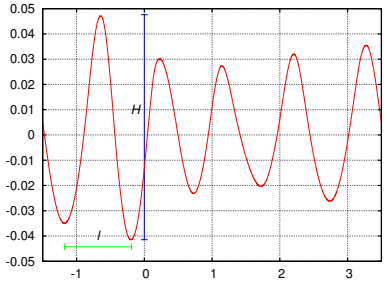

Figure 3: Sketch of the way used to compute the wave height and the wavelength for the calculation of the maximum wave steepness.

Among the many open questions concerning the breaking generated by the modulational instability, an important question is when the breaking ends. As an attempt of answering this question, at each time step the maximum wave steepness is computed. Several definitions exist for that parameter, which depends on how the wavelength and the wave amplitude are defined. In this work the maximum steepness is computed as the maximum of the quantity

$$\epsilon = \frac{H}{2}\frac{2\pi}{l}$$

where H is the vertical distance between the crest and the trough at the right whereas l is the distance between the two troughs next to the crest (see Fig. 3).

In Fig. 4 the time histories of the maximum wave steepness are plotted together with the corresponding energy contents in water. The threshold steepness of 0.32 discussed in Grue and Fructus (2010) and in Iafrati (2009) is also drawn. Although simulations IV and VI are still going, the results indicate that the breaking starts when a limiting steepness is reached and ceases once the steepness drops below the threshold value. Note that once the breaking ceases the energy dissipation rate takes about the same slope of the pre-breaking phase. These conclusions are essentially similar to what was found for a gentle spilling breaking in Iafrati (2011). It is worth noticing that the reduction of the wave steepness shown in Fig. 4 is only partly related to the reduction in the wave amplitude whereas a important role is played by the downshifting phenomenon. This is clearly seen in Fig. 2 where the peak of the spectrum moves from $k = 10.47$ m^{-1} to $k = 8.37$ m^{-1}.

Before closing this section, it is worth providing a few additional considerations on the time histories of the maximum steepness provided in Fig. 4. The maximum steepness oscillates with a period of about 5 nondimensional units, which is twice the wave period. As already discussed, this is a consequence of the interaction between the wave components and the group envelope. A second remark concerns the peak values of the steepness reached during the breaking process for which numerical results predict maximum values exceeding 0.55. In Toffoli *et al.* (2010), the value 0.55 was found to be a limiting steepness for oceanic waves. It is not clear at the moment if the larger values found here are caused by the way in which the maximum steepness is computed during the breaking event when the free surface takes quite complicated shapes. Further studies are needed to clarify this aspect.

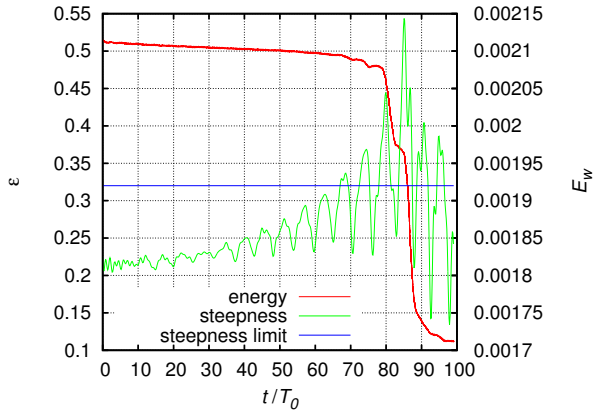

a)

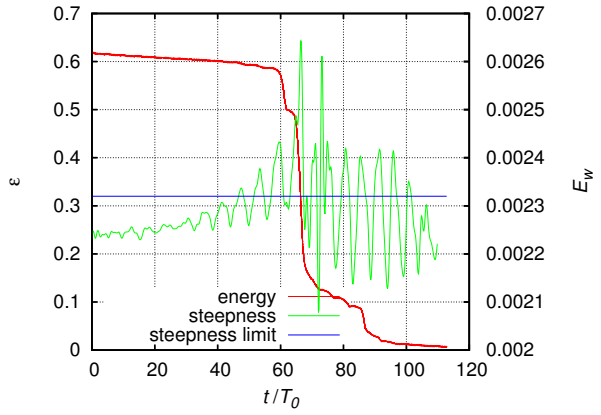

b)

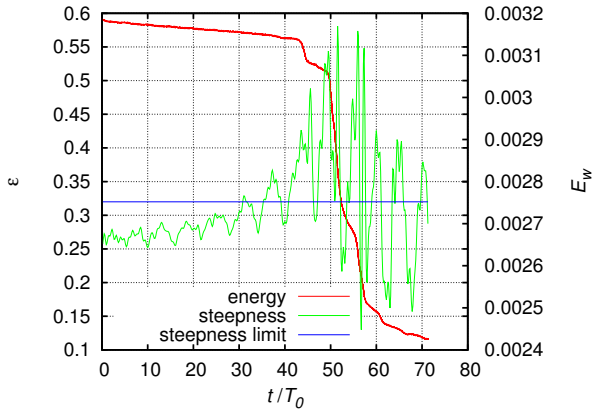

c)

Figure 4: Time histories of the maximum wave steepness and of the total energy content in water for the three different steepnesses: a) case IV ($\epsilon_0 = 0.18$), b) case V ($\epsilon_0 = 0.20$), c) case VI ($\epsilon_0 = 0.22$). The horizontal line indicate the threshold steepness of 0.32.

4. ACKNOWLEDGMENTS

The work has been financially supported by the "Flagship Project RITMARE - The Italian Research for the Sea - coordinated by the Italian National Research Council and funded by the Italian Ministry of Education, University and Research within the National Research Program 2011-2013." Authors express their gratitude to the Gerris team and Dr. S. Popinet not only for making the code available but also for the technical support provided.

5. REFERENCES

M. Perlin, W. Choi, Z. Tian, (2013) Breaking waves in deep and intermediate waters. Annu. Rev. Fluid Mech., 45, pp. 115-145.

A.V. Babanin, T. Waseda, T. Kinoshita, A. Toffoli, (2011) Wave breaking in directional fields. J. Phys. Oceanogr., 41, pp. 145-156.

R.J. Rapp, W.K. Melville, (1990) Laboratory measurements of deep-water breaking waves. Philos. Trans. R. Soc. A, 331, pp. 735-800.

A.D. Drazen, W.K. Melville, L. Lenain, (2008) Inertial scaling of dissipation in unsteady breaking waves, J. Fluid Mech., 611, pp. 307-332.

J. Grue, D. Clamond, M. Huseby, A. Jensen, A. (2003) Kinematics of extreme water waves. Appl. Ocean Res. 25, pp. 355-366.

M. Donelan, M.S. Longuet-Higgins, J.S. Turner, (1972) Periodicity in whitecaps. Nature, 239, pp. 449-451.

T. Lamont-Smith, J. Fuchs, M.P. Tulin, (2003) Radar Investigation of the Structure of Wind Waves. J. Oceanogr., 59, pp. 49-63.

W. Xiao, Y. Liu, G. Wu, D.K.P. Yue, (2013) Rogue wave occurrence and dynamics by direct simulations of nonlinear wave-field evolution. J. Fluid Mech., 720, pp. 357-392.

A. Iafrati, M. Onorato, A. Babanin, (2012) Analysis of wave breaking events generated as a result of a modulational instability. Proc. 29th ONR Symposium on Naval Hydrodynamics, Gothenburg, Sweden.

A. Iafrati, A. Babanin, M. Onorato, (2013) Modulational instability, wave breaking, and formation of large-scale dipoles in the atmosphere. Phys. Rev. Lett., 110, 184504.

A. Iafrati, A. Babanin, M. Onorato, (2014) Modeling of oceanatmosphere interaction phenomena during the breaking of modulated wave trains. J. Comput. Phys., 271, pp. 151-171.

M. Landrini, O. Oshri, T. Waseda, M.P. Tulin, (1998) Long time evolution of gravity wave system. Proc. 13th Int. Workshop Water Waves Floating Bodies, Alphen aan den Rijn, Netherlands.

S. Popinet, (2009) An accurate adaptive solver for surface-tension-driven interfacial flows. J. Comput. Phys., 228, pp. 5838-5866.

M.P. Tulin, T. Waseda, (1999) Laboratory observations of wave group evolution, including breaking effects. J. Fluid Mech., 378, 197-232.

J. Grue, D. Fructus, (2010) Model for fully nonlinear ocean wave simulations derived using Fourier inversion of integral equations in 3D. Advances in Numerical Simulation of Nonlinear Water Waves (ed. Q. W. Ma), in the series of Advances in Coastal and Ocean Engineering. World Scientific.

A. Iafrati, (2011) Energy dissipation mechanisms in wave breaking processes: spilling and highly aerated plunging breaking events. J. Geophys. Res. 116, C07024

A. Toffoli, A. Babanin, M. Onorato, T. Waseda, (2010) Maximum steepness of oceanic waves: Field and laboratory experiments. Geophys. Res. Lett., L05603, doi:10.1029/2009GL041771.